Dark matter constraints on low mass and weakly coupled $B-L$ gauge boson

Rabindra N. Mohapatra[1] and Nobuchika Okada[2]

[1]*Maryland Center for Fundamental Physics and Department of Physics, University of Maryland, College Park, Maryland 20742, USA*

[2]*Department of Physics and Astronomy, University of Alabama, Tuscaloosa, Alabama 35487, USA*

(Received 16 April 2020; accepted 13 August 2020; published 27 August 2020)

We investigate constraints on the new $B-L$ gauge boson (Z_{BL}) mass and coupling (g_{BL}) in a $U(1)_{B-L}$ extension of the standard model (SM) with an SM singlet Dirac fermion (ζ) as dark matter (DM). The DM particle ζ has an arbitrary $B-L$ charge Q chosen to guarantee its stability. We focus on the small Z_{BL} mass and small g_{BL} regions of the model, and find new constraints for the cases where the DM relic abundance arises from thermal freeze-out as well as freeze-in mechanisms. In the thermal freeze-out case, the dark matter coupling is given by $g_\zeta \equiv g_{BL}Q \simeq 0.016\sqrt{m_\zeta[\mathrm{GeV}]}$ to reproduce the observed DM relic density and $g_{BL} \geq 2.7\times 10^{-8}\sqrt{m_\zeta[\mathrm{GeV}]}$ for the DM particle to be in thermal equilibrium prior to freeze-out. Combined with the direct dark matter detection constraints and the indirect constraints from cosmic microwave background and AMS-02 measurements, discussed in earlier papers, we find that the allowed mass regions are limited to be $m_\zeta \gtrsim 200$ GeV and $M_{Z_{BL}} \gtrsim 10$ GeV. We then discuss the lower g_{BL} values where the freeze-in scenario operates and find the following relic density constraints on parameters depending on the g_{BL} range and dark matter mass: Case (A): for $g_{BL} \geq 2.7\times 10^{-8}\sqrt{m_\zeta[\mathrm{GeV}]}$, one has $g_\zeta^2 g_{BL}^2 + \frac{0.82}{1.2} g_\zeta^4 \simeq 8.2\times 10^{-24}$; and Case (B): for $g_{BL} < 2.7\times 10^{-8}\sqrt{m_\zeta[\mathrm{GeV}]}$, there are two separate constraints depending on m_ζ. Case (B1): for $m_\zeta \lesssim 2.5$ TeV, we find $g_\zeta^2 g_{BL}^2 \simeq 8.2\times 10^{-24}(\frac{m_\zeta}{2.5\ \mathrm{TeV}})$; and Case (B2): for $m_\zeta \gtrsim 2.5$ TeV, we have $g_\zeta^2 g_{BL}^2 \simeq 8.2\times 10^{-24}$. For this case, we display the various parameter regions of the model that can be probed by a variety of "Lifetime Frontier" experiments such as FASER, FASER2, Belle II, SHiP, and LDMX.

DOI: 10.1103/PhysRevD.102.035028

I. INTRODUCTION

Extensions of the standard model (SM) with $U(1)_{B-L}$ as a possible new symmetry of electroweak interactions are well motivated due to their connections to the neutrino mass [1,2] and have recently attracted a great deal of attention. Theoretical constraints of anomaly cancellation allow two classes of $B-L$ extensions: (i) one motivated by left-right symmetric and SO(10) models, where the $B-L$ generator contributes to the electric charge of particles [1–3] and (ii) another, where it does not [4–10]. The second alternative is not embeddable into the left-right or SO(10) models. Both classes of models require the addition of three right-handed neutrinos to satisfy the anomaly constraints and lead to the seesaw mechanism for neutrino masses [11–15]. There is, however, a fundamental difference between the two classes of models as regards the possible magnitudes of their gauge couplings: in the first class of models where the $B-L$ contributes to the electric charge [1–3], there is a relation between the electric charge of the positron and the $B-L$ gauge coupling:

$$\frac{1}{e^2} = \frac{1}{g_L^2} + \frac{1}{g_R^2} + \frac{1}{g_{BL}^2}. \tag{1}$$

As a result, there is a lower bound on the value of g_{BL}:

$$\frac{1}{g_{BL}^2} \leq \frac{\cos^2\theta_W}{e^2} \quad \text{or} \quad g_{BL} \geq 0.34. \tag{2}$$

This lower bound gets strengthened to 0.416, when it is assumed that all $U(1)$ couplings in the $SU(2)_L \times U(1)_{I_{3R}} \times U(1)_{B-L}$ model are perturbative till the grand unified theory scale [16].

In the second class of models, on the other hand, there is no lower bound on g_{BL} from theoretical considerations, and as a result, it can be arbitrarily small. In this paper, we focus on this class of models in the small g_{BL} and small $B-L$ gauge boson mass ($M_{Z_{BL}}$) regions to see what kinds of phenomenological constraints exist, once we add a Dirac

dark matter fermion ζ to the theory. We let the dark matter (DM) field have an arbitrary $B-L$ charge, Q. Clearly, it is possible to choose a $B-L$ charge Q for ζ so that it is naturally stable as is required for a dark matter particle. For example, if we choose Q to be a half odd integral value, there are no operators in the theory that will make it decay. This class of models is completely realistic as far as its fermion sector is concerned. There are four parameters: g_{BL}, $g_\zeta \equiv g_{BL}Q$ plus the two mass parameters, m_ζ and $M_{Z_{BL}}$, which enter into our dark matter discussion. See Refs. [17,18] for the case where the two mass parameters are in the multi-TeV range. We keep the masses arbitrary and find constraints on them in our model. Although our interest is mostly phenomenological in this paper and therefore we do not worry about the origin and naturalness of small gauge couplings, we do note that small gauge couplings are motivated by a class of large volume compactification of string theories (see, for example, Ref. [19]). We also ignore mixings between the $B-L$ gauge boson and the SM gauge bosons as well as the mixing between Z_{BL} and the photon, for simplicity. As a result, there are no mixing effects in the Z_{BL} couplings. In any case, these mixing effects are loop suppressed and therefore smaller than the effects we have considered. The DM particle, ζ, in our case is a Dirac fermion, as just mentioned, and the gauge anomaly cancellation is automatically satisfied. To emphasize again, ζ is stable due to the choice of its $B-L$ charge.

We discuss constraints that g_{BL} and g_ζ must satisfy from the requirements that the particle ζ be a viable dark matter; i.e., it satisfies the relic density constraints as well as direct detection constraints and other indirect detection constraints such as from cosmic microwave background (CMB) and cosmic ray measurements. We consider the following two gauge coupling parameter ranges of the theory: (i) one where the DM relic density arises via thermal freeze-out, and (ii) the second case where the couplings, g_{BL} and g_ζ, are so small that the DM particle ζ was never in thermal equilibrium in the early universe with SM particles, and it had a vanishing density at the reheating after inflation. The DM relic abundance in the latter case was built up via the freeze-in mechanism [20–23]. In the first case, we find that the relic density constraint requires that $g_\zeta \simeq 0.016\sqrt{m_\zeta[\mathrm{GeV}]}$ and the condition for thermal equilibrium of Z_{BL} in the early universe requires that $g_{BL} \gtrsim 2.7\times 10^{-8}\sqrt{m_\zeta[\mathrm{GeV}]}$. For the freeze-in case, we find that the product $g_{BL}g_\zeta \approx 2.9\times 10^{-12}$ to satisfy the constraint of the DM relic density. This result is independent of the dark matter mass as long as $m_\zeta \gtrsim 2.5$ TeV $\gg M_{Z_{BL}}$. When the dark matter mass is less than 2.5 TeV, the so-called sequential freeze-in mechanism dominates and the condition on couplings becomes $g_{BL}g_\zeta \approx 2.9\times 10^{-12}\sqrt{m_\zeta/2.5\ \mathrm{TeV}}$ (the freeze-in mechanism for a Majorana fermion DM and $g_\zeta = g_{BL}$ was investigated in Ref. [24] and their results are consistent with ours). It is interesting that the spin-independent direct detection cross section also depends on the product $(g_{BL}g_\zeta)^2\mu_{\zeta N}^2/M_{Z_{BL}}^4$ (where $\mu_{\zeta N}$ is the reduced mass of the DM-nucleon system), and therefore the Ω_{DM} constraint also puts lower limits on the Z_{BL} mass. We explain the origin of these constraints and elaborate on the details in the body of the paper.

We next comment on two more cases: Case (iiiA) where the g_ζ is large enough that both Z_{BL} and ζ were in equilibrium with each other but not with the SM particles; and Case (iiiB) where both $g_{\zeta,BL}$ are so small that all three sectors were thermally sequestered from each other. These cases do not fall into either the freeze-in or the freeze-out scenarios and are therefore listed separately.

There are also constraints on this model from Fermi-LAT observations that assume 100% branching ratio to either $b\bar{b}$ or $\tau^+\tau^-$ [25], which are compatible with the thermal freeze-out constraints only for $m_\zeta \geq$ few GeV. The assumption of 100% branching ratio is, however, not the case for our model, and we have more like 20% for the branching ratio. As a result, our bounds are weaker, and we estimate it to be in the 2 GeV range for the freeze-out case using Fig. 9 of the Fermi-LAT paper [25].

We note here that there are other $B-L$ models with dark matter in the literature [26,27] as well as $B-L$ models without the dark matter [28]. There are also models with dark photon [29] and dark $U(1)$ models [30] with some similarity to $B-L$ models. Our model is, however, different from all of them. For example, Ref. [28] discusses constraints g_{BL} and $M_{Z_{BL}}$ for a pure $B-L$ model with Dirac neutrinos without any dark matter, whereas not only does our model have a dark matter but also the neutrinos are Majorana particles which obtain their mass from the seesaw mechanism resulting from $B-L$ breaking. Furthermore, we consider the case where the $B-L$ gauge boson couples to the dark matter having an arbitrary $B-L$ charge. As far as Ref. [27] is concerned, it uses the lightest right-handed neutrino as the dark matter and as a result, its $B-L$ charge of DM is fixed by anomaly cancellation. On the other hand, in our model, the dark fermion is separate from the usual SM plus the right-handed neutrinos model. As a result, we can choose its $B-L$ charge arbitrarily consistent with anomaly cancellation. This allows us to explore a very different range of parameters of the $B-L$ model. Our model is also different from other $U(1)$ based models, e.g., Refs. [29,30], although they have some similarity to our discussion, e.g., their constraints on dark photon portal models with an MeV dark matter (see Ref. [29]). We have used some results from this paper, e.g., the CMB bounds on dark matter using Fig. 3 of Ref. [29] which imply the constraint of dark matter mass of $m_\zeta \geq 1$ GeV. To be consistent with the bounds, in this paper, we focus on the region of dark matter mass, $m_\zeta \geq 1$ GeV.

The paper is organized as follows: in Sec. II, we outline the details of the model. In Sec. III, we discuss the case of

thermal freeze-out of the dark matter and the constraints on the relevant model parameters from it. We then combine it with the already existing indirect detection constraints to find new allowed regions for the DM mass for different $M_{Z_{BL}}$ values. In Sec. IV, we switch to the parameter range of the model where the relic density arises out of the freeze-in mechanism and the constraints implied by it on the model. We note how the FASER experiment [31] combined with other planned/proposed experiments such as Belle II, SHiP, and LDMX can probe the parameter range of the model. We also comment on constraints from the SN1987A and big bang nucleosynthesis (BBN). In Sec. V, we briefly discuss the case where the "dark sector" with ζ and Z_{BL} is decoupled from the SM thermal plasma and is produced from the inflaton decay at the end of inflation. We conclude in Sec. VI with a discussion of implications of our results and some additional comments.

II. THE $B-L$ MODEL WITH DIRAC FERMION DARK MATTER

A. Model details

Our model is based on the $U(1)_{B-L}$ extension of the SM with gauge quantum numbers under $U(1)_{B-L}$ defined by their baryon or lepton number of particles. The gauge group of the model is $SU(3)_c \times SU(2)_L \times U(1)_Y \times U(1)_{B-L}$, where Y is the SM hypercharge. We need three right-handed neutrinos (RHNs) with $B-L=-1$ to cancel the $B-L$ anomaly. The RHNs being SM singlets do not contribute to SM anomalies. The electric charge formula in this case is the same as in the SM. We now add to this model a vectorlike SM singlet fermion ζ with $B-L$ charge equal to Q. Being vectorlike, this fermion does not affect the anomaly cancellation of the model. The $B-L$ group is assumed not to contribute to the electric charge formula as stated in the Introduction. As a result, its couplings are theoretically not restricted. We assume that there is a Higgs boson with $B-L=+2$ which gives a Majorana mass to the RHNs, thereby helping to implement the seesaw mechanism for neutrino masses since the SM Higgs doublet already provides the Dirac mass to the neutrinos. The interaction Lagrangian in our model describing the interaction of the $B-L$ gauge boson (called Z_{BL} here) is

$$\mathcal{L}_{Z_{BL}} = (Z_{BL})_\mu \left[g_{BL} \sum_f (B-L)_f \bar{f}\gamma^\mu f + g_\zeta \bar{\zeta}\gamma^\mu \zeta \right]. \quad (3)$$

This Lagrangian is enough to derive our conclusions. We start with letting the values of g_{BL}, $g_\zeta \equiv Q g_{BL}$, $M_{Z_{BL}}$, and m_ζ as free parameters and explore the smaller mass range of $M_{Z_{BL}}$, and as a benchmark point, we take m_ζ in the range of 1 GeV to few TeV range with $M_{Z_{BL}} < m_\zeta$. Clearly this covers a wide and interesting range of dark matter masses.

B. New Higgs bosons and other phenomenology

The only new Higgs boson in the model beyond the SM Higgs doublet is an SM singlet field Δ with $B-L=2$. It acquires a nonzero vacuum expectation value $\langle \Delta \rangle = v_{BL}$. The real part of Δ is a physical Higgs field, which we denote by σ. It couples to the right-handed neutrinos which we assume are heavy (in the TeV range or higher) so that σ could be a long-lived particle. Also it has no direct couplings to quarks and leptons, and such couplings arise from its mixing with the SM Higgs boson. For a GeV mass σ, we may expect this mixing to be of order $m_\sigma^2/m_h^2 \sim 10^{-2}$. Due to this small coupling, its production cross section in lepton as well as hadron colliders is very small. Further discussion of the phenomenology of this new Higgs boson is beyond the scope of this paper. In fact, in a recent paper [32], we have argued that for some parameter ranges of the theory, the σ particle can be a decaying dark matter of the universe.

As far as other phenomenology of the model is concerned, we note that for $g_{BL}^2/M_{Z_{BL}}^2 \lesssim 10^{-6}$ GeV^{-2}, the neutral current and other low energy constraints are automatically satisfied (see Table 8.13 of Ref. [33]). This limit broadly satisfies all the LEP constraints for VV type current couplings. It also implies that $g_{BL} \lesssim 10^{-3} M_{Z_{BL}}$[GeV] is allowed by low energy observations, and we seek other constraints in this domain when a dark matter is included in the theory. There are also ATLAS upper bounds on g_{BL} as a function of $M_{Z_{BL}}$ but this bound for low mass Z_{BL} is in the range of $g_{BL} \leq 2 \times 10^{-3}$ or so [34] for $M_{Z_{BL}}$ about a GeV, and it becomes weaker as we go to higher masses. See also the review [35].

We also note that our model is different from other $U(1)'$ models since in our case the Z_{BL} coupling with quarks and leptons is specified by the $B-L$ charges of the fermions. On the other hand, the DM field has an arbitrary $B-L$ charge Q, and we investigate the phenomenological viability of our model for a wide range of the parameter space from $|Q| \ll 1$ to $|Q| \gg 1$.

III. CASE (I): THERMAL DARK MATTER CONSTRAINTS

A. Dark matter relic density

We first consider the case where the parameter range of the model is such that ζ is a thermal dark matter. We will find these parameter ranges and their possible implications below. This is the case where both g_{BL} and g_ζ have such values that Z_{BL}, ζ, and SM particles were all in thermal equilibrium in the early universe, followed by the dark matter decoupling which leads to the DM relic density.

We first note that the dark matter interacts with the SM particle only via the $B-L$ gauge interactions. The Higgs boson field that breaks $B-L$ does not couple to the dark matter particle due to their $B-L$ charge mismatch and

therefore does not contribute to the thermal equilibrium consideration between ζ and SM particles.

For the Dirac DM particle ζ to be a thermal dark matter, whose relic abundance is determined by thermal freeze-out, it must be in thermal equilibrium with the SM particles as well as the Z_{BL} in the very early universe. As the temperature of the universe drops below the m_ζ, the Boltzmann suppression makes the ζ particle density low and it goes out of equilibrium. After thermal freeze-out occurs, the DM freely expands till the current epoch and forms the dark matter of the universe. Its current abundance is determined by the values of g_{BL}, g_ζ, and m_ζ.

Typically in a thermal freeze-out situation, the fact that at one point the ζ particle was in equilibrium implies constraints on the parameters g_ζ. We have to consider different processes that can keep ζ particles in equilibrium with the SM particles. The first one is via direct process $\zeta\bar{\zeta} \to f\bar{f}$ mediated by Z_{BL}, which leads to

$$n_\zeta(T)\langle\sigma v\rangle_{\zeta\bar{\zeta}\to f\bar{f}} \geq H = \sqrt{\frac{\pi^2}{90}g_*}\frac{T^2}{M_P}, \tag{4}$$

where $n_\zeta(T) = \frac{3\zeta(3)}{\pi^2}T^3$ is the DM number density for $T \gtrsim m_\zeta$, g_* is the effective number of degrees of freedom for SM particles in thermal equilibrium (we set $g_* = 106.75$ in the following analysis), and $M_P = 2.43 \times 10^{18}$ GeV is the reduced Planck mass. Since we are interested in a low mass Z_{BL} boson, we obtain $\langle\sigma v\rangle \simeq \frac{g_{BL}^2 g_\zeta^2}{4\pi T^2}$ for the $\zeta\bar{\zeta} \to f\bar{f}$ process, independently of the Z_{BL} mass. Requiring the thermal equilibrium condition to be satisfied at $T \simeq m_\zeta$, we obtain the following constraint on the gauge coupling parameters:

$$g_{BL}^2 g_\zeta^2 \geq 43\frac{m_\zeta}{M_P}. \tag{5}$$

As we will see in the next subsection, the above thermal equilibrium condition is not consistent with the direct DM detection constraints which are very severe for low $M_{Z_{BL}}$.

The second possibility for ζ to be in equilibrium with the SM particles is via a two step process: in the first step Z_{BL} comes to equilibrium with SM fermions via the process $f\bar{f} \to Z_{BL}\gamma$ and then ζ goes into equilibrium with Z_{BL} and hence with the SM fermions via the process $Z_{BL}Z_{BL} \to \zeta\zeta$. The thermal equilibrium condition for the first process is

$$n_{Z_{BL}}(T)\langle\sigma v\rangle_{f\bar{f}\to Z_{BL}\gamma} \geq H = \sqrt{\frac{\pi^2}{90}g_*}\frac{T^2}{M_P}, \tag{6}$$

where $n_{Z_{BL}}(T) = \frac{2\zeta(3)}{\pi^2}T^3$ is the number density of Z_{BL}, and $\langle\sigma v\rangle_{f\bar{f}\to Z_{BL}\gamma} \simeq \frac{g_{BL}^2\alpha_e}{T^2}$ with the fine-structure constant of $\alpha_e = 1/128$. We require that this condition is satisfied at $T = m_\zeta$ (at the latest) and obtain

$$g_{BL} \geq 2.7 \times 10^{-8}\sqrt{m_\zeta[\mathrm{GeV}]}. \tag{7}$$

The second process depends only on g_ζ, and the equilibrium condition gives a lower bound on $g_\zeta \geq 9.2 \times 10^{-5}(m_\zeta[\mathrm{GeV}])^{1/4}$ by using $\langle\sigma v\rangle_{Z_{BL}Z_{BL}\to\zeta\bar{\zeta}} \simeq \frac{g_\zeta^4}{16\pi T^2}$ in Eq. (4). Clearly if we want to get the DM relic density right, we need a larger g_ζ; and therefore it is in our acceptable range for the DM relic density, and ζ is in thermal equilibrium with Z_{BL}. Note that the processes $Z_{BL} \to ff$ and $ff \to Z_{BL}$, which apparently are not suppressed by electromagnetic coupling, are expected to be phase space suppressed instead; so we do not consider them here.

Next, we discuss the DM relic density constraints on the model. To evaluate the DM relic density, we solve the Boltzmann equation given by

$$\frac{dY}{dx} = -\frac{\langle\sigma v\rangle}{x^2}\frac{s(m_\zeta)}{H(m_\zeta)}(Y^2 - Y_{\mathrm{EQ}}^2), \tag{8}$$

where $x = m_\zeta/T$ is the inverse "temperature" normalized by the DM mass m_ζ, $\langle\sigma v\rangle$ is a thermally averaged DM annihilation cross section (σ) times relative velocity (v), $H(m_\zeta)$ is the Hubble parameter at $T = m_\zeta$, $s(m_\zeta)$ is the entropy density of the thermal plasma at $T = m_\zeta$, Y is the yield of the DM particle which is defined as a ratio of the DM number density to the entropy density, and Y_{EQ} is the yield of the DM in thermal equilibrium. Explicit forms for the quantities in the Boltzmann equation are as follows:

$$\begin{aligned} H(m_\zeta) &= \sqrt{\frac{\pi^2}{90}g_*}\frac{m_\zeta^2}{M_P}, \\ s(m_\zeta) &= \frac{2\pi^2}{45}g_* m_\zeta^3, \\ Y_{\mathrm{EQ}}(x) &= \frac{g_{\mathrm{DM}}}{2\pi^2}\frac{x^2 m_\zeta^3}{s(m_\zeta)}K_2(x), \end{aligned} \tag{9}$$

where $K_2(x)$ is the modified Bessel function of the second kind and $g_{\mathrm{DM}} = 4$ is the number of degrees of freedom for the Dirac fermion DM particle ζ.

The thermal average of the DM annihilation cross section is given by the following integral expression:

$$\langle\sigma v\rangle = \frac{g_{\mathrm{DM}}^2}{64\pi^4}\left(\frac{m_\zeta}{x}\right)\frac{1}{n_{\mathrm{EQ}}^2}\int_{4m_\zeta^2}^{\infty} ds(\sigma v)s\sqrt{s-4m_\zeta^2}K_1\left(\frac{x\sqrt{s}}{m_\zeta}\right), \tag{10}$$

where $n_{\mathrm{EQ}} = s(m_\zeta)Y_{\mathrm{EQ}}/x^3$ is the DM number density, and K_1 is the modified Bessel function of the first kind. The DM annihilation occurs via the process $\zeta\bar{\zeta} \to Z_{BL}Z_{BL}$ for $m_\zeta > M_{Z_{BL}}$. In our considerations above, we have ignored

the inverse decay process $\zeta\bar{\zeta} \to Z_{BL}$, since it is a small contribution at high temperatures, suppressed by a very small volume of the phase space. We have also not taken into account the Sommerfeld enhancement. Typically, Sommerfeld enhancement is significant if the DM speed is very low and bound states of ζ-$\bar{\zeta}$ are formed with a large g_ζ value. In our freeze-out scenario, the annihilation cross section in the early universe uses the speed $v \sim 0.05$ or so and the coupling is not so large [see Eq. (13)]. Similarly, the condition for DM bound state formation is not satisfied. We estimate the Sommerfeld enhancement factor to be therefore small at the freeze-out epoch. However, at the recombination and the current epoch, the Sommerfeld effect is significant due to very low velocities of DM particles and leads to important constraints on the parameters for the freeze-out case (see below). By solving the Boltzmann equation of Eq. (8) with the initial condition $Y(x) = Y_{\rm EQ}(x)$ for $x \ll 1$, we evaluate the DM yield at present, $Y(x \to \infty)$. The relic abundance of the DM in the present universe is then given by

$$\Omega_{\rm DM}h^2 = \frac{m_\zeta s_0 Y(\infty)}{\rho_c/h^2}, \tag{11}$$

where $s_0 = 2890\ {\rm cm}^{-3}$ is the entropy density of the present universe and $\rho_c/h^2 = 1.05 \times 10^{-5}\ {\rm GeV/cm}^3$ is the critical density. For the thermal DM scenario, the asymptotic solution of the Boltzmann equation $[Y(\infty)]$ is known, and with a good accuracy, the thermal DM relic density is expressed to be [36,37]

$$\Omega_{\rm DM}h^2 \simeq \frac{2.13 \times 10^8 x_f}{\sqrt{g_*}M_P\langle\sigma v\rangle}, \tag{12}$$

where M_P and $\langle\sigma v\rangle$ are evaluated in units of GeV and the freeze-out temperature of the DM particle is approximately evaluated as $x_f = m_\zeta/T_f \simeq \ln(x) - 0.5\ln(\ln(x))$ with $x \simeq 0.19\sqrt{g_{\rm DM}/g_*}M_P m_\zeta\langle\sigma v\rangle$. Since the annihilation process occurs via s wave, we can approximate $\langle\sigma v\rangle$ as σv in the nonrelativistic limit. Here in our analysis, we employ Eqs. (A5) and (A2) given in Appendix for the annihilation processes $\zeta\bar{\zeta} \to Z_{BL}Z_{BL}$ and $\zeta\bar{\zeta} \to f\bar{f}$, respectively. As we will discuss in the following subsection, the direct DM detection constraints are very severe, and we find that they require $g_{BL} \ll g_\zeta$. Thus, the contribution from the process $\zeta\bar{\zeta} \to f\bar{f}$ is negligibly small.

In order to reproduce the observed DM relic density at the present epoch, $\Omega_{\rm DM}h^2 = 0.12$ [38], we obtain a relation between the DM mass and the DM coupling with Z_{BL} for $M^2_{Z_{BL}} \ll m^2_\zeta$, which is shown by the line in Fig. 1. The observed DM relic density is reproduced along the line, which we find to be well approximated by

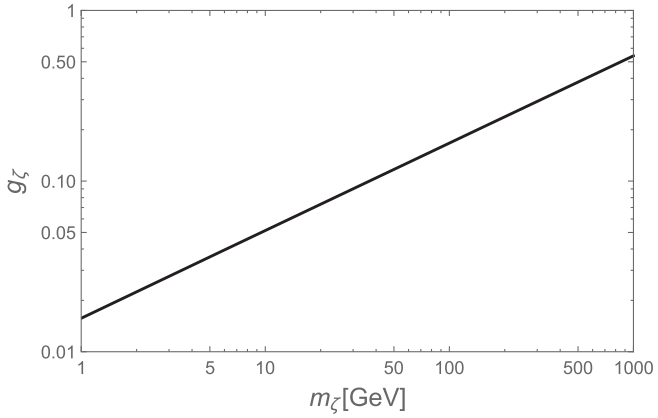

FIG. 1. The relation between the DM mass and the DM coupling with Z_{BL} for the case of $M^2_{Z_{BL}} \ll m^2_\zeta$. The observed DM relic density is reproduced along the line. $g_\zeta \simeq 0.016 \times \sqrt{m_\zeta[{\rm GeV}]}$ is a good approximation formula.

$$g_\zeta \simeq 0.016 \times \sqrt{m_\zeta[{\rm GeV}]}. \tag{13}$$

As we expected, the thermal equilibrium condition for the process $Z_{BL}Z_{BL} \leftrightarrow \zeta\bar{\zeta}$ we have found before [see after Eq. (7)] is always satisfied for $m_\zeta > 1$ GeV. In Fig. 2, we show the relation between the Z_{BL} mass and the DM coupling with Z_{BL} for fixed DM masses of 2 GeV (black line), 10 GeV (red line), 100 GeV (blue line), and 500 GeV

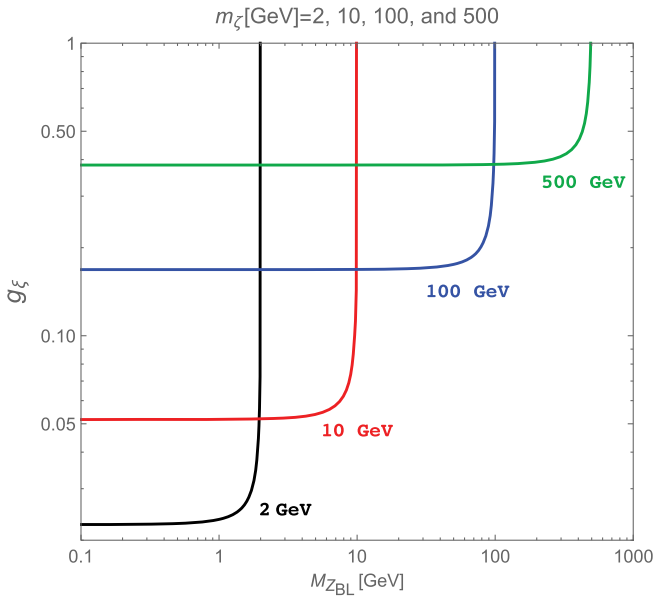

FIG. 2. The relation between the Z_{BL} mass and the DM coupling with Z_{BL} for fixed DM masses of 2 GeV (black line), 10 GeV (red line), 100 GeV (blue line), and 500 GeV (green line). The observed DM relic density is reproduced along each line. For $M^2_{Z_{BL}} \ll m^2_\zeta$, the coupling is almost constant for a fixed DM mass. The coupling rises sharply when the Z_{BL} mass becomes very close to the DM mass because of the phase space effect.

(green line). The observed DM relic density is reproduced along each line. We can see that the coupling is almost constant for a fixed DM mass for $M_{Z_{BL}}^2 \ll m_\zeta^2$ and is well approximated by Eq. (13). The coupling is sharply rising when the Z_{BL} mass becomes very close to the DM mass because of the phase space/kinematic effect.

B. Direct detection constraints

Let us now turn to the direct detection constraints. In Fig. 3, we show the current upper bound on the spin-independent cross section ($\sigma_{\rm SI}$) for the elastic scattering of the DM particle with a nucleon for the DM mass of $m_{\rm DM} \geq 2$ GeV. For the DM mass $m_{\rm DM} \geq 6$ GeV, the most stringent upper bound is obtained by XENON1T experiment [39] while for 2 GeV $\leq m_{\rm DM} \leq 6$ GeV, the upper bound is obtained by a combination of DarkSide-50 [40], LUX [41], and PandaX-II [42]. As is well known the constraints are most severe for a DM mass around 30 GeV and become weaker on either side of this mass.

In our model, the elastic scattering of the DM particle with a nucleon $\zeta N \to \zeta N$ occurs via the exchange of the Z_{BL} boson. The cross section for the process is given by [43]

$$\sigma_{\rm SI} = \frac{1}{\pi} g_\zeta^2 g_{BL}^2 \frac{\mu_{\zeta N}^2}{M_{Z_{BL}}^4}, \tag{14}$$

where $\mu_{\zeta N} = m_\zeta m_N/(m_\zeta + m_N)$ is the reduced mass for the DM-nucleon system with $m_N = 0.983$ GeV being the nucleon mass. Note that this cross section formula is valid for $M_{Z_{BL}}^2 \gtrsim M_T E_R$, where M_T is a target nuclei mass and E_R is a typical recoil energy. For XENON1T experiment, $M_T \sim 100$ GeV and $E_R \sim 10$ keV, so that we can apply Eq. (14) for $M_{Z_{BL}} \gtrsim 50$ MeV. As $M_{Z_{BL}}$ decreases from $M_{Z_{BL}} = 50$ MeV, the Z_{BL} exchange process becomes long-range and $\sigma_{\rm SI}$ quickly approaches a constant value as shown in Refs. [44–47]. For $M_{Z_{BL}} < 50$ MeV, we approximate the constant cross section by Eq. (14) with $M_{Z_{BL}} = 50$ MeV fixed. For a given m_ζ, say, 1 GeV, which satisfies all the above constraints, we see that as $M_{Z_{BL}}$ goes down, the cross section rises in Eq. (14). Since g_{BL} has a lower bound from Eq. (7) and g_ζ values are already fixed, this implies a lower bound on $M_{Z_{BL}}$ depending on the ζ mass along the upper bound on $\sigma_{\rm SI}$ in Fig. 3. This lower bound is shown as the black solid line in Fig. 4. For example, for $m_\zeta = 2$ GeV, we find the minimum Z_{BL} mass to be $\simeq$50 MeV.

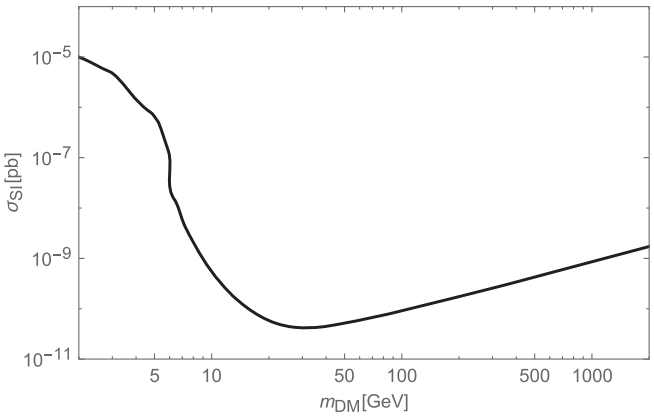

FIG. 3. The current experimental upper bound on the spin-independent cross section as a function of the DM mass.

C. Indirect detection constraints

In our model, the dark matter annihilation to $Z_{BL}Z_{BL}$ at late time can undergo Sommerfeld enhancement due to the low velocity of the DM fermion. The Z_{BL}'s can subsequently decay to SM fermions, which can lead to signals in indirect DM searches such as the CMB measurement and AMS-02 antiproton searches. These constraints have been analyzed in Refs. [30,48], and they lead to very tight constraints on the DM mass in the range of 1 GeV to 100 GeV. Even though Ref. [30] considers a dark photon portal, it is very similar to our $B-L$ portal, and therefore

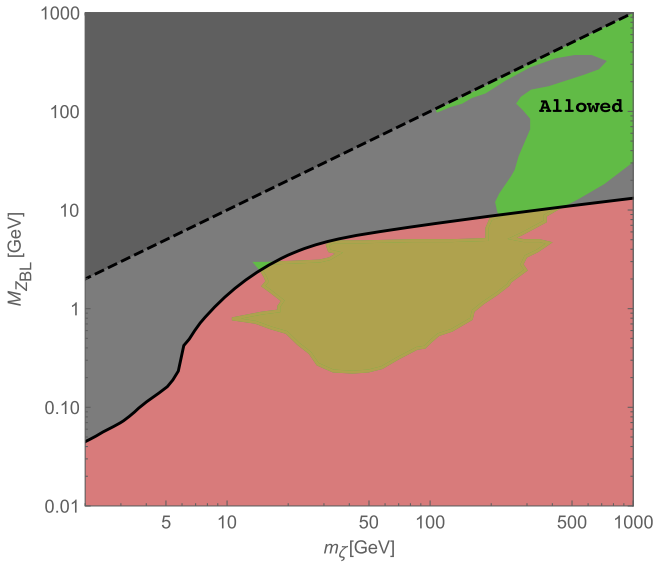

FIG. 4. The parameter regions in the $(m_\zeta, M_{Z_{BL}})$ plane that satisfy the conditions from the spin-independent cross section bounds and the indirect detection constraints obtained in Ref. [30], as well as the condition for the thermal equilibrium between Z_{BL} and the SM particles. The region below the solid black line is disallowed by the spin-independent cross section constraints and the thermal equilibrium between Z_{BL} and the SM particles. The region above the dashed line, which corresponds to $m_\zeta \leq m_{Z_{BL}}$, is not considered in the paper. The gray region is ruled out by indirect constraints from the CMB data and the AMS-02 results [30]. The yellowish looking region is the extension of the green region, and only the tip of it sticks out in the middle of the figure. The allowed region for the freeze-out case then turns out to be the green region, i.e., $m_\zeta \gtrsim 100$ GeV and $M_{Z_{BL}} \gtrsim 10$ GeV.

we can apply their constraints to our case. In Fig. 4, we have combined the direct detection constraint with the indirect detection constraints obtained in Ref. [30]. The green region is allowed by all the constraints, and this pretty much rules out the low mass (thermal) DM scenario for $m_{Z_{BL}} \lesssim 10$ GeV.

IV. CASE (II): FREEZE-IN DARK MATTER SCENARIO

In this case, we require the dark matter fermion ζ not to be in equilibrium with either the SM particles or the Z_{BL}. There are then several constraints on the couplings g_{BL} and g_ζ that emerge in this case if ζ has to play the role of dark matter. We discuss them below.

A. Dark matter relic density

This case arises when the gauge couplings g_{BL} and g_ζ have much smaller values than the freeze-out case so that the dark matter particle was never in equilibrium with the thermal plasma of the SM particles. In this section, we assume that the ζ particle had zero initial abundance at the reheating after inflation. Productions of ζ particles from inflaton decay will be briefly discussed in Sec. V. There are then two possible cases:

(A) the Z_{BL} was in thermal equilibrium with SM particles. This corresponds to the case where $g_{BL} \geq 2.7 \times 10^{-8}\sqrt{m_\zeta[\mathrm{GeV}]}$, and

(B) the Z_{BL} was not in thermal equilibrium with SM particles, i.e., $g_{BL} < 2.7 \times 10^{-8}\sqrt{m_\zeta[\mathrm{GeV}]}$.

For Case (A), we find that the most conservative conditions for the reaction $\zeta\bar{\zeta} \leftrightarrow f\bar{f}$ to be out of equilibrium till the BBN epoch is

$$g_{BL} g_\zeta \leq 10^{-10}. \tag{15}$$

This follows for $M_{Z_{BL}} \leq 1$ GeV, requiring that the above reaction falls out of equilibrium above the $T = 1$ GeV epoch of the universe. For higher Z_{BL} masses, the condition is even weaker. Similarly, for DM mass in the low GeV range, there is Boltzmann suppression in its number density and the bound becomes weaker as well. Similarly, for the process $\zeta\bar{\zeta} \leftrightarrow Z_{BL}Z_{BL}$, the corresponding condition is

$$g_\zeta \leq 9.2 \times 10^{-5}(m_\zeta[\mathrm{GeV}])^{1/4}. \tag{16}$$

Next, we proceed to evaluate the DM relic abundance by numerically solving the Boltzmann equation in Eq. (8). Note that even for the freeze-in case the Boltzmann equation is of the same form as in the thermal dark matter case. This is because the term proportional to Y_{EQ}^2 in the right-hand side of Eq. (8) corresponds to the DM particle productions from the SM thermal plasma. The difference from the thermal dark matter case is that we set the boundary condition for the freeze-in case to be $Y(x_{\mathrm{RH}}) = 0$, where $x_{\mathrm{RH}} = m_\zeta/T_{\mathrm{RH}} \ll 1$ is related to the reheat temperature (T_{RH}) after inflation. The relic abundance of the DM in the present universe is given in Eq. (11).

In evaluating the thermal average of the DM annihilation cross section in Eq. (10), we consider two processes for the DM particle creation, $f\bar{f} \to \zeta\bar{\zeta}$ mediated by Z_{BL} and $Z_{BL}Z_{BL} \to \zeta\bar{\zeta}$. Note that the second process is active only for Case (A) (except for a special case, sequential freeze-in, that we discuss below). The corresponding cross sections are given by those of the DM annihilation processes. In Appendix, we list the exact cross section formulas for the processes. Using them for Eq. (10), we evaluate the thermal average of the cross section and then numerically solve the Boltzmann equation of Eq. (8) with the boundary condition of $Y(x_{\mathrm{RH}}) = 0$. In the freeze-in mechanism, the DM particles are created mostly in the relativistic regime, $T \gg m_\zeta$, where the annihilation cross sections are approximately given by [see Eqs. (A3) and (A6) in Appendix]

$$\sigma(\bar{\zeta}\zeta \to f\bar{f})v \simeq \frac{37}{36\pi s} g_\zeta^2 g_{BL}^2,$$
$$\sigma(\bar{\zeta}\zeta \to Z_{BL}Z_{BL})v \simeq \frac{g_\zeta^4}{4\pi s}\left(\ln\left[\frac{s}{m_\zeta^2}\right] - 1\right), \tag{17}$$

where we have assumed $m_b^2 \ll m_\zeta^2 < m_t^2$ and $m_{Z_{BL}}^2 \ll m_\zeta^2$. Although we use the exact cross section formulas to evaluate $Y(x)$ in our analysis, we find that the approximation formulas in Eq. (17) lead to almost the same results as those obtained by the exact formulas.

In Fig. 5, fixing $m_\zeta = 30$ GeV, we show the resultant $Y(x)$ for two cases: One is for $g_\zeta^2 g_{BL}^2 = 8.2 \times 10^{-24}$ with

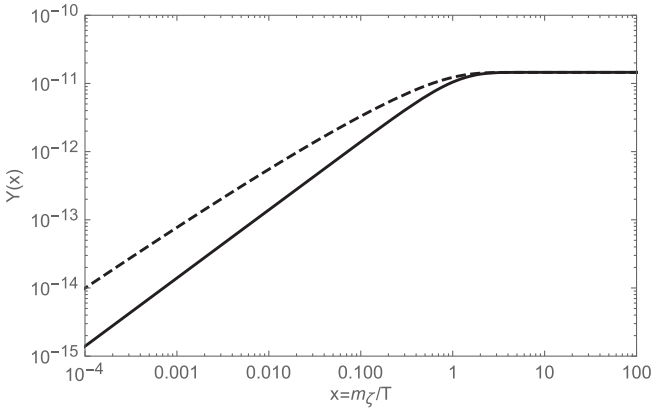

FIG. 5. The yield of the Dirac DM particle as a function of $x = m_\zeta/T$ for $m_\zeta = 30$ GeV. The solid line denotes the result for $g_\zeta^2 g_{BL}^2 = 8.2 \times 10^{-24}$ with $g_{BL}^2 \gg g_\zeta^2$, while the dashed line denotes the result for $g_\zeta^4 = 1.2 \times 10^{-23}$ with $g_{BL}^2 \ll g_\zeta^2$. In both cases, $\Omega_{\mathrm{DM}}h^2 = 0.12$ is reproduced. In this analysis, we have used the exact formulas for the annihilation cross sections given in Appendix.

$g_{BL} \gg g_\zeta$ (solid line), and the other is $g_\zeta^4 = 1.2 \times 10^{-23}$ with $g_{BL} \ll g_\zeta$ (dashed line). For the first case, the process $\zeta\bar{\zeta} \to f\bar{f}$ dominates, while the process $\zeta\bar{\zeta} \to Z_{BL}Z_{BL}$ dominates for the second case. As we can see, $Y(x)$ grows from $Y(x_{\rm RH} \ll 1) = 0$ and becomes constant at $x \simeq 1$. Using the approximation formulas in Eq. (17), this behavior can be qualitatively understood as follows: In the first case, for $x \lesssim 1$, we have $\langle\sigma v\rangle \propto g_\zeta^2 g_{BL}^2 (x^2/m_\zeta^2)$, and Eq. (8) can easily be solved with $Y \ll Y_{\rm EQ} \simeq$ constant and $Y(x_{\rm RH} \ll 1) = 0$. We find a solution to be $Y(x) \propto g_\zeta^2 g_{BL}^2 (x - x_{\rm RH})/m_\zeta \simeq g_\zeta^2 g_B^2 (x/m_\zeta)$. Since the DM particle creation from the thermal plasma should stop at $T \sim m_\zeta$ because of the kinematics, $Y(\infty) \sim Y(x \simeq 1) \propto g_\zeta^2 g_{BL}^2/m_\zeta$. Using Eq. (11), we find that the resultant DM relic density is proportional to $g_\zeta^2 g_B^2$ while independent of the DM mass. We have arrived at the same conclusion even for the numerical result by using the exact cross section formulas. We find a similar result for the second case; namely, the resultant DM relic density is proportional to g_ζ^4 while independent of the DM mass.

By numerically solving the Boltzman equation, we find that independently of m_ζ, the observed DM relic density of $\Omega_{\rm DM}h^2 = 0.12$ is reproduced in Case (A) by

$$g_\zeta^2 g_{BL}^2 + \frac{0.82}{1.2} g_\zeta^4 \simeq 8.2 \times 10^{-24} \quad \text{for} \quad g_{BL} \geq 2.7 \times 10^{-8} \sqrt{m_\zeta[\text{GeV}]}. \tag{18}$$

In Case (B), on the other hand, there is no Z_{BL} initially, the condition is given by only the first term in the above equation, i.e.,

$$g_\zeta^2 g_{BL}^2 \simeq 8.2 \times 10^{-24} \quad \text{for } g_{BL} < 2.7 \times 10^{-8} \sqrt{m_\zeta[\text{GeV}]}. \tag{19}$$

For example, for $m_\zeta = 1$ GeV, the first equation implies that $g_\zeta \sim 10^{-6}$ or lower, whereas the second case corresponds to $g_\zeta \sim 10^{-4}$ or higher.

Very recently, it has been pointed out in Ref. [49] that in Case (B) "sequential freeze-in" can dominantly produce the DM particles compared to the process of $f\bar{f} \to \zeta\bar{\zeta}$ considered above. If this is the case, Eq. (19) is not the right condition to reproduce $\Omega_{\rm DM}h^2 = 0.12$. In the case of sequential freeze-in, the DM particles are produced in two steps. First, Z_{BL} is produced from the thermal plasma of the SM particles, and then the DM particles are produced through $Z_{BL}Z_{BL} \to \zeta\bar{\zeta}$. Let us now estimate the DM relic density through the sequential freeze-in. The yield of Z_{BL} ($Y_{Z_{BL}}$) is calculated by the Boltzmann equation,

$$\frac{dY_{Z_{BL}}}{dx} \simeq \frac{\langle\sigma v\rangle_{f\bar{f}\to Z_{BL}\gamma}}{x^2} \frac{s(m_\zeta)}{H(m_\zeta)} Y_{Z_{BL}}^{\rm EQ} Y_\gamma^{\rm EQ}, \tag{20}$$

where $Y_{Z_{BL}}^{\rm EQ} \simeq Y_\gamma^{\rm EQ} \simeq 5.2 \times 10^{-3}$ are the yields of Z_{BL} and the photon, respectively, in the thermal equilibrium, and $\langle\sigma v\rangle_{f\bar{f}\to Z_{BL}\gamma} \simeq \frac{g_{BL}^2 \alpha_e}{m_\zeta^2} x^2$. This Boltzmann equation is easily solved from $x_{\rm RH} \ll 1$, and we find

$$Y_{Z_{BL}}(x) \simeq 2.9 \times 10^{-6} \left(\frac{M_P}{m_\zeta}\right) g_{BL}^2 x \tag{21}$$

for $x \lesssim m_\zeta/M_{Z_{BL}}$. With this $Y_{Z_{BL}}(x)$, we calculate the DM density by solving the Boltzmann equation,

$$\frac{dY}{dx} \simeq \frac{\langle\sigma v\rangle_{Z_{BL}Z_{BL}\to\zeta\bar{\zeta}}}{x^2} \frac{s(m_\zeta)}{H(m_\zeta)} Y_{Z_{BL}}^2 = \frac{\langle\sigma v\rangle_{\zeta\bar{\zeta}\to Z_{BL}Z_{BL}}}{x^2} \frac{s(m_\zeta)}{H(m_\zeta)} Y_{\rm EQ}^2 \left(\frac{Y_{Z_{BL}}}{Y_{Z_{BL}}^{\rm EQ}}\right)^2, \tag{22}$$

where we have used $\langle\sigma v\rangle_{Z_{BL}Z_{BL}\to\zeta\bar{\zeta}} (Y_{Z_{BL}}^{\rm EQ})^2 = \langle\sigma v\rangle_{\zeta\bar{\zeta}\to Z_{BL}Z_{BL}} Y_{\rm EQ}^2$ in the second line. In our analysis here, we have assumed that the sequential freeze-in dominates and neglected the DM pair production process $f\bar{f} \to \bar{\zeta}\zeta$ from the thermal plasma.

For fixed values of g_{BL}, g_ζ, and m_ζ, we numerically solve Eq. (22) from $x_{\rm RH} \ll 1$. In Fig. 6, we show the yield of the Dirac DM particle as a function of $x = m_\zeta/T$ for $m_\zeta = 30$ GeV (solid line), along with the yield of Z_{BL} (dashed line). Here, we have taken $g_{BL} = 5.0 \times 10^{-10}$ and $g_\zeta = 6.3 \times 10^{-4}$. We can see the result similar to that in Fig. 5. As we can understand from Eq. (21) and Eq. (A4), $Y(\infty) \sim Y(x = 1) \propto g_\zeta^4 g_{BL}^4/m_\zeta^2$. We find that the observed DM relic density of $\Omega_{\rm DM}h^2 = 0.12$ is reproduced when

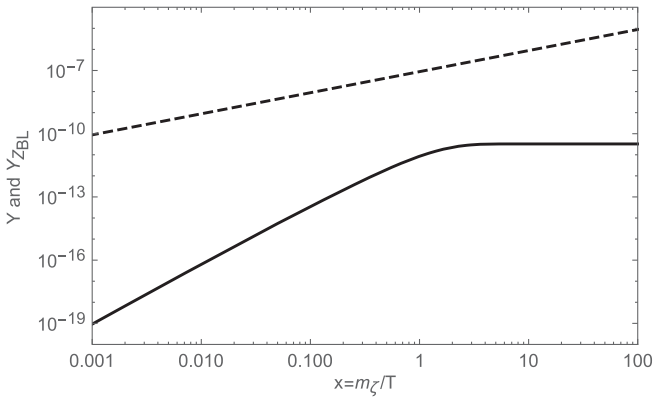

FIG. 6. In the sequential freeze-in case, the yield of the Dirac DM particle as a function of $x = m_\zeta/T$ for $m_\zeta = 30$ GeV (solid line), along with the yield of Z_{BL} (dashed line). Here, we have taken $g_{BL} = 5.0 \times 10^{-10}$ and $g_\zeta = 6.3 \times 10^{-4}$, by which $\Omega_{\rm DM}h^2 = 0.12$ is reproduced.

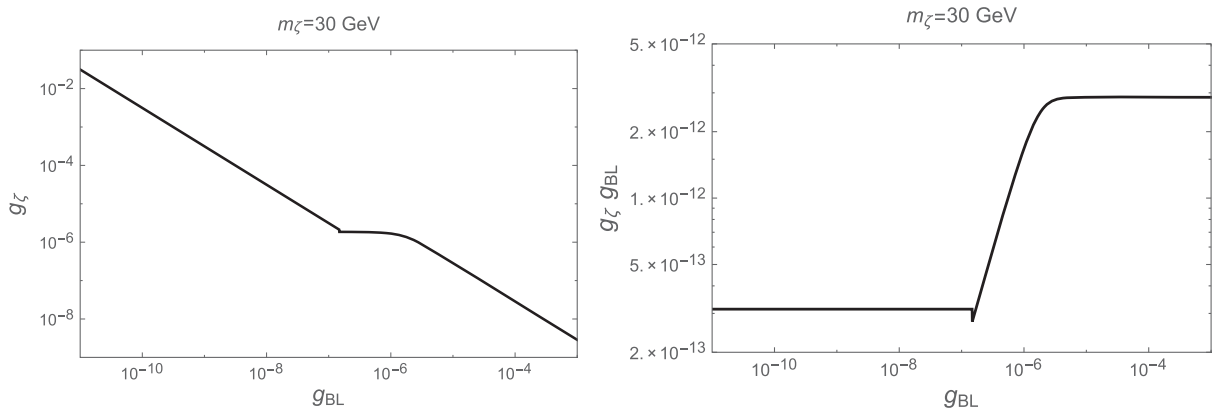

FIG. 7. The plot of g_ζ vs g_{BL} (left panel) and $g_\zeta g_{BL}$ vs g_{BL} (right panel) for $m_\zeta = 30$ GeV. The observed DM relic density is reproduced along the solid lines. Note that since we have analyzed Case (A) and Case (B) separately, the discontinuity appears at $g_{BL} \simeq 1.5 \times 10^{-7}$ for $m_\zeta = 30$ GeV, where Z_{BL} goes out of/in thermal equilibrium with the SM particles.

$$g_\zeta^2 g_{BL}^2 \simeq 8.2 \times 10^{-24} \left(\frac{m_\zeta}{2.5\ \text{TeV}}\right). \tag{23}$$

Comparing this result with Eq. (19), we conclude that the sequential freeze-in dominantly produces the DM particles for $m_\zeta < 2.5$ TeV, in Case (B). For $m_\zeta = 30$ GeV, our result is displayed in Fig. 7. The plots show cusps at $g_{BL} \simeq 1.5 \times 10^{-7}$, which is the boundary value to separate Case (A) and Case (B). To simplify our analysis, we have calculated the two cases separately by considering only the dominant process in each case. Because of this simplification, the cusps appear in our results, and they will be smoothed away if we take all terms into account in the Boltzmann equations.

Thus to summarize, for the freeze-in scenario, there are the following constraints on parameters to reproduce the observed DM relic density depending on the ranges of $B-L$ gauge coupling g_{BL} and dark matter mass m_ζ. Case (A): This constraint applies for the parameter region $g_{BL} \geq 2.7 \times 10^{-8}\sqrt{m_\zeta[\text{GeV}]}$ where one has $g_\zeta^2 g_{BL}^2 + \frac{0.82}{1.2} g_\zeta^4 \simeq 8.2 \times 10^{-24}$ to reproduce $\Omega_{\text{DM}} h^2 = 0.12$. Case (B): for $g_{BL} < 2.7 \times 10^{-8}\sqrt{m_\zeta[\text{GeV}]}$, there are two separate constraints depending on m_ζ. Case (B1): for $m_\zeta \lesssim 2.5$ TeV, we find $g_\zeta^2 g_{BL}^2 \simeq 8.2 \times 10^{-24}(\frac{m_\zeta}{2.5\ \text{TeV}})$; and in Case (B2): for $m_\zeta \gtrsim 1.5$ TeV, we find $g_\zeta^2 g_{BL}^2 \simeq 8.2 \times 10^{-24}$.

B. Possible laboratory probes of the freeze-in case

We now discuss possible probes of the freeze-in scenario in the laboratory. There are several experiments that can probe various parameter ranges of the model. This is shown in Fig. 8. The relevant experiments are those attempting to extend the lifetime frontier of various new weakly coupled beyond the SM particles. They typically look for displaced vertices. The experiments are FASER and SHiP at the

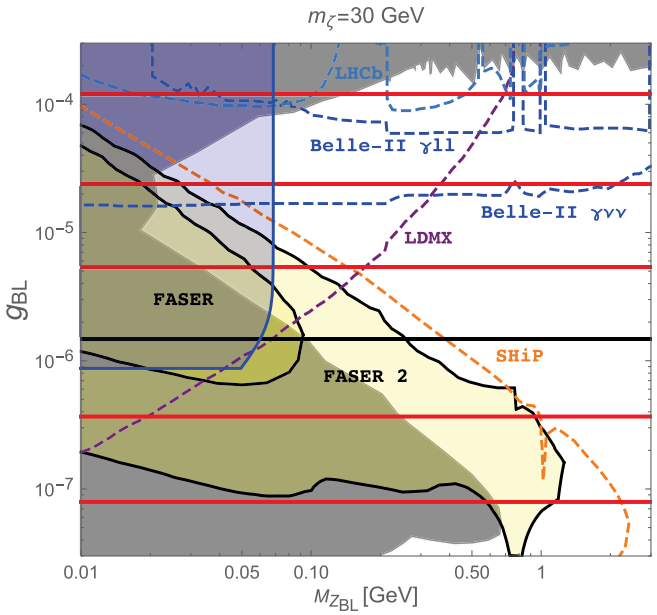

FIG. 8. The various horizontal lines, along which $\Omega_{\text{DM}} h^2 = 0.12$ is reproduced, show the results for various Q values: $Q = 2 \times 10^{-4}$, 5×10^{-3}, 0.1, 1.01 (black line), 5, and 50 from top to bottom. We go vertically up as Q decreases [see Eqs. (18) and (23)]. Here, we have chosen $m_\zeta = 30$ GeV. Reaches of the various experiments are shown in different color lines. FASER and FASER 2 in solid black lines. Orange dashed line is for SHiP [50], purple dashed line for LDMX [51], dark-blue dashed lines for Belle II [52], and light-blue dashed lines for LHCb [53,54]. The region to the left of the solid blue line is excluded by the XENON1T results. The line is vertical because $g_{BL} g_\zeta$ is almost constant for $g_{BL} \gtrsim 10^{-6}$ (see the right panel in Fig. 7) in Eq. (18). For $M_{Z_{BL}} \lesssim 50$ MeV, σ_{SI} becomes independent of $M_{Z_{BL}}$ [44–47], and the XENON1T bound is satisfied for $g_{BL} g_\zeta \lesssim 1.5 \times 10^{-12}$. This means that the XENON1T constraint is always satisfied for $g_{BL} \lesssim 8.9 \times 10^{-7}$ in our scenario.

LHC; Belle II andLHCb as well as LDMX experiment proposed to search for weakly coupled light DM particles.

The planned FASER detector [55] at the LHC will probe the low $M_{Z_{BL}}$ ($\leq$ 1–2 GeV) and low g_{BL} region of the theory. This is a detector which will be installed in a tunnel near the ATLAS detector about 480 meters away to look for displaced vertices with charged particles from long-lived charge-neutral particles produced at the primary LHC vertex. In the very low g_{BL} range, our model falls into this category since due to low g_{BL} and low mass $M_{Z_{BL}}$, the distance traveled by a highly boosted Z_{BL} before decaying is given by $c\tau \sim \frac{12\pi E_{Z_{BL}}}{g_{BL}^2 M_{Z_{BL}}^2}$, and experiments such as FASER searching for displaced vertices can give useful constraints.

In Fig. 8, the horizontal solid lines correspond to the results for the various $B-L$ charges of the DM particle, $Q = 2\times10^{-4}$, 5×10^{-3}, 0.1, 1.01 (black line), 5, and 50 from top to bottom. Along the horizontal lines, $\Omega_{\rm DM}h^2 = 0.12$ is satisfied. Various planned and proposed experiments and their search reaches are indicated (see Ref. [55] for details) and the current excluded region is gray-shaded [56]. The blue shaded region at the top-left corner is excluded by the XENON1T results. As discussed in Sec. III B, $\sigma_{\rm SI}$ becomes constant for $M_{Z_{BL}} \lesssim 50$ MeV, and we find that the XENON1T bound is satisfied for $g_{BL} \lesssim 8.9\times10^{-7}$ for any values of $M_{Z_{BL}}$. Even for the freeze-in case, the direct DM detection experiments provide very severe constraints and exclude a part of the open window. From Fig. 8, we see that various Lifetime Frontier experiments in the near future can test our freeze-in scenario.

C. Astrophysical and BBN constraints on low mass Z_{BL}

If Z_{BL} mass is less than 100 MeV, it can be produced from e^+e^- and $\nu\bar{\nu}$ collisions in the supernova, whose core temperature is believed to be 30 MeV. To avoid any constraints on g_{BL} from energy loss considerations of SN 1987A, we stay above Z_{BL} mass of 200 MeV.

Coming to constraints from big bang nucleosynthesis, we assume that the RHNs required for anomaly cancellation acquire heavy Majorana mass ($M_{N_R} \geq 100$ GeV or more) so that the only new degree of freedom we have to consider at the epoch of BBN are the three modes of the vector boson Z_{BL} (two transverse and one longitudinal). We assume $M_{Z_{BL}}$ to be in the 1 GeV or lower range but above 200 MeV. For the higher mass range, as long as Z_{BL} is in thermal equilibrium, the Z_{BL} density at decoupling is already suppressed enough so that there are no BBN constraints.

The physics of our considerations in the lower mass range are as follows: if the gauge coupling is large enough that the Z_{BL} is in thermal equilibrium till $T = 1$ MeV, then how much it contributes to the quantity $\Delta N_{\rm eff}$ depends on its mass. If its mass is larger than 10 MeV, its abundance at $T = 1$ MeV will be Boltzmann suppressed and its contributions to energy density will be within the current $\Delta N_{\rm eff}$ limits. Since we are interested in the mass range of 200 MeV or more to avoid supernova constraints, we need not worry about the BBN constraints unless the gauge coupling is below 10^{-10} GeV in which case it can survive till $T \sim 1$ MeV and affect BBN. The limit of 10^{-10} comes from requiring that $\Gamma_{Z_{BL}} \sim H(T = 1\ {\rm MeV})$.

V. CASE (III): SMALL g_{BL} AND SECLUDED DARK SECTOR WITH ζ AND Z_{BL}

In this section we briefly comment on two more logical possibilities which arise when $g_{BL} < 2.7\times10^{-8}\sqrt{m_\zeta[{\rm GeV}]}$ so that the SM particles are decoupled from the ζ and Z_{BL} sectors. There are two possibilities here: Case (iiiA) where g_ζ is large enough so that the DM particle can be in equilibrium with Z_{BL} but not with the SM sector due to small g_{BL}; and Case (iiiB) where g_ζ is small so that all three sectors are sequestered. Here we comment briefly on how the relic density can arise in both of the cases.

In either of cases (iiiA) and (iiiB), the decay of the inflaton will play a crucial role in building up the DM relic density. Assuming the inflaton ϕ being a gauge singlet scalar under the SM and $B-L$ gauge groups, we can consider couplings of the inflaton with particles in our model such as $c_H\phi H^\dagger H$, $c_\zeta\phi\bar{\zeta}\zeta$, and $c_Z\phi\mathcal{Z}_{BL}^{\mu\nu}\mathcal{Z}_{BL\,\mu\nu}$, where H is the SM Higgs doublet, $\mathcal{Z}_{BL}^{\mu\nu}$ is the field strength of Z_{BL}, c_H is a coupling with a mass dimension $+1$, c_ζ is a dimensionless coupling, and c_Z is a coupling with a mass dimension -1. After the end of inflation, the inflaton decays to particles through these couplings to reheat the universe, and then the big bang Hubble era begins. Assuming that the inflaton is much heavier than any other particles, the inflaton partial decay widths are calculated as

$$\Gamma_{\phi\to H^\dagger H} = \frac{c_H^2}{8\pi m_\phi},$$
$$\Gamma_{\phi\to\bar{\zeta}\zeta} = \frac{c_\zeta^2}{8\pi} m_\phi,$$
$$\Gamma_{\phi\to Z_{BL}Z_{BL}} = \frac{c_Z^2}{4\pi} m_\phi^3. \tag{24}$$

We consider that the inflaton mainly decays to the Higgs doublets and the reheating temperature (of the SM particle plasma) is estimated by $\Gamma_{\phi\to H^\dagger H} \simeq H(T_{\rm RH})$, so that

$$T_{\rm RH} \simeq \sqrt{\Gamma_{\phi\to H^\dagger H} M_P} \sim c_H\sqrt{\frac{M_P}{m_\phi}}. \tag{25}$$

For case (ii) in Sec. IV, we implicitly assumed that the branching ratio of the inflaton decay into the DM particles is negligibly small so that we employed the initial condition

$Y(x_{\rm RH}) = 0$ in solving the Boltzmann equation. Here in case (iii), we are considering the case where the inflaton branching ratio into the "dark sector" with ζ and Z_{BL} is not negligible. There are then two possible cases.

For case (iiiA), the early universe after reheating consists of two separate plasmas: one is the thermal plasma of the SM particles and the other is the plasma of the hidden sector, where ζ and Z_{BL} are in thermal equilibrium. Note that the formula to evaluate the reheating temperature, $\Gamma_{\phi\to H^\dagger H} \simeq H(T_{\rm RH})$, means that the inflaton energy at its lifetime is transmitted to the SM particles plasma. Thus, we estimate the reheating temperature of the dark sector by

$$T_{\rm RH}^{\text{dark sector}} \simeq \sqrt{\Gamma_{\phi\to H^\dagger H} M_P} \times \sqrt{{\rm BR}(\phi\to\bar{\zeta}\zeta) + {\rm BR}(\phi\to Z_{BL}Z_{BL})}, \tag{26}$$

where ${\rm BR}(\phi\to\bar{\zeta}\zeta)$ and ${\rm BR}(\phi\to Z_{BL}Z_{BL})$ are the inflaton branching ratios to $\bar{\zeta}\zeta$ and $Z_{BL}Z_{BL}$, respectively. Although the temperatures of the SM sector and the dark sector are not the same, unless the branching ratio is extremely small, the evaluation of the DM relic density is similar to Case (i) discussed in Sec. III.

For Case (iiiB), on the other hand, all three sectors are sequestered. The energy density of the dark matter sector at the reheating is estimated by

$$\rho_\zeta \simeq {\rm BR}(\phi\to\bar{\zeta}\zeta)\times\rho_{\rm rad}(T_{\rm RH}), \tag{27}$$

where $\rho_{\rm rad} = \frac{\pi^2}{30} g_* T_{\rm RH}^4$ is the energy density of the SM particle plasma. For a given $T_{\rm RH}$ value, we may adjust the inflaton branching ratio into a pair of DM particles to reproduce the observed DM relic density.

As a final comment, we note that one may identify the inflaton field with the $B-L$ breaking Higgs boson (Δ). In this case, we consider couplings of the inflaton such as $\lambda_{\rm mix}\Delta^\dagger\Delta H^\dagger H$, $\frac{c_\Delta}{M_P}\Delta^\dagger\Delta\bar{\zeta}\zeta$, and $g_{BL}^2\Delta^\dagger\Delta Z_{BL}^\mu Z_{BL\,\mu}$, where $\lambda_{\rm mix}$ and c_Δ are dimensionless coupling constants. We can apply the above discussion by the replacements: $\phi\to\sigma$, $c_H\to\lambda_{\rm mix}v_{BL}$, $c_\zeta\to v_{BL}/M_P$, and $c_Z\to g^2 v_{BL}$.

VI. SUMMARY AND CONCLUSIONS

In summary, we have considered an extension of the standard model with the gauged $U(1)_{B-L}$ symmetry and a Dirac fermion with arbitrary $B-L$ charge which plays the role of dark matter. The $B-L$ symmetry is broken by a $B-L=2$ Higgs field so that Z_{BL} picks up a mass and it leads to the seesaw mechanism for neutrino masses. This provides a unified picture of neutrinos and dark matter. Ignoring the mixings of Z_{BL} with SM gauge bosons, we show that in the weakly coupled $B-L$ gauge boson case there are constraints on the gauge couplings g_{BL} of SM fermions and g_ζ of dark matter as well as the masses of the dark matter and $M_{Z_{BL}}$ from different observations such as Fermi-LAT, CMB, $\Omega_{\rm DM}h^2$, and direct dark matter detection experiments for the case when the dark matter is a thermal freeze-out type. We also point out that for even weaker gauge couplings where the dark matter relic density arises via the freeze-in mechanism, there are constraints on the above couplings from the observed dark matter relic density as well as from the supernova 1987A observations. We note that parts of the freeze-in parameter range of the model can be tested in the FASER experiment being planned at the LHC and other Lifetime Frontier experiments.

ACKNOWLEDGMENTS

N. O. thanks the Maryland Center for Fundamental Physics for hospitality during his visit. The work of R. N. M. is supported by the National Science Foundation Grants No. PHY1620074 and No. PHY-1914631, and the work of N. O. is supported by the U.S. Department of Energy Grant No. DE-SC0012447.

Note added.—After this work was put in the arXiv, the paper arXiv:1908.09834 [57] with a similar study was brought to our attention.

APPENDIX: DARK MATTER ANNIHILATION CROSS SECTIONS TO VARIOUS FINAL STATES

In this appendix, we list the formulas that we have used in our analysis.

For the annihilation process of $\zeta\bar{\zeta}\to Z_{BL}\to f\bar{f}$, the cross section times relative velocity is given by

$$\sigma v = \frac{g_\zeta^2 g_{BL}^2}{6\pi s}\sum_f N_c^f Q_f^2 \frac{(s+2m_\zeta^2)(s+2m_f^2)}{(s-M_{Z_{BL}}^2)^2}\sqrt{1-\frac{4m_f^2}{s}}, \tag{A1}$$

where f denotes a SM fermion with mass of m_f, Q_f is its $B-L$ charge, and N_c^f is the color number in the final state of a SM fermion: $N_c^f=3$ for a quark, $N_c^f=1$ for a charged lepton, and $N_c^f=1/2$ for a SM neutrino ($m_f\to 0$). Since we are interested in the case of $m_\zeta > M_{Z_{BL}}$, we have neglected the decay width of the Z_{BL} boson in the above formula. In the nonrelativistic limit, the cross section formula is simplified to be

$$\sigma v \simeq \frac{g_\zeta^2 g_{BL}^2}{2\pi}\sum_f N_c^f Q_f^2 \frac{2m_\zeta^2+m_f^2}{(4m_\zeta^2-M_{Z_{BL}}^2)^2}\sqrt{1-\frac{m_f^2}{m_\zeta^2}}, \tag{A2}$$

while in the relativistic limit,

$$\sigma v \simeq \frac{g_\zeta^2 g_{BL}^2}{6\pi s}\sum_f N_c^f Q_f^2. \tag{A3}$$

For the annihilation process of $\zeta\bar{\zeta} \to Z_{BL}Z_{BL}$, the cross section times relative velocity is given by

$$\sigma v = \frac{g_\zeta^4}{4\pi s}\sqrt{1-\frac{4m_{Z_{BL}}^2}{s}} \times \left(-1 - \frac{(2+a^2)^2}{(2-a^2)^2+4b^2} + \frac{6-2a^2+a^4+12b^2+4b^4}{2bc(1+b^2+c^2)}\ln\left[\frac{1+(b+c)^2}{1+(b-c)^2}\right]\right), \tag{A4}$$

where $a = \frac{M_{Z_{BL}}}{m_\zeta}$, $b = \sqrt{\frac{s}{4m_\zeta^2}-1}$, and $c = \sqrt{\frac{s}{4m_\zeta^2}-a^2}$. In the nonrelativistic limit, this cross section formula is simplified to be

$$\sigma v \simeq \frac{g_\zeta^4}{16\pi m_\zeta^2}\left(1-\frac{M_{Z_{BL}}^2}{m_\zeta^2}\right)^{3/2}\left(1-\frac{M_{Z_{BL}}^2}{2m_\zeta^2}\right)^{-2}, \tag{A5}$$

while in the relativistic limit,

$$\sigma v \simeq \frac{g_\zeta^4}{4\pi s}\left(\ln\left[\frac{s}{m_\zeta^2}\right]-1\right). \tag{A6}$$

[1] R. E. Marshak and R. N. Mohapatra, Phys. Lett. **91B**, 222 (1980).
[2] R. N. Mohapatra and R. E. Marshak, Phys. Rev. Lett. **44**, 1316 (1980).
[3] A. Davidson, Phys. Rev. D **20**, 776 (1979).
[4] W. Buchmuller, C. Greub, and P. Minkowski, Phys. Lett. B **267**, 395 (1991).
[5] S. Khalil, J. Phys. G **35**, 055001 (2008).
[6] L. Basso, arXiv:1106.4462.
[7] L. Basso, A. Belyaev, S. Moretti, and C. H. Shepherd-Themistocleous, Phys. Rev. D **80**, 055030 (2009).
[8] S. Iso, N. Okada, and Y. Orikasa, Phys. Lett. B **676**, 81 (2009); Phys. Rev. D **80**, 115007 (2009).
[9] A. A. Abdelalim, A. Hammad, and S. Khalil, Phys. Rev. D **90**, 115015 (2014).
[10] A. Biswas, S. Choubey, and S. Khan, J. High Energy Phys. 08 (2018) 062.
[11] P. Minkowski, Phys. Lett. **67B**, 421 (1977).
[12] R. N. Mohapatra and G. Senjanović, Phys. Rev. Lett. **44**, 912 (1980).
[13] T. Yanagida, Conf. Proc. C **7902131**, 95 (1979).
[14] M. Gell-Mann, P. Ramond, and R. Slansky, Conf. Proc. C **790927**, 315 (1979).
[15] S. L. Glashow, NATO Sci. Ser. B **61**, 687 (1980).
[16] G. Chauhan, P. S. B. Dev, R. N. Mohapatra, and Y. Zhang, J. High Energy Phys. 01 (2019) 208.
[17] P. Fileviez Perez, C. Murgui, and A. D. Plascencia, Phys. Rev. D **100**, 035041 (2019).
[18] P. H. Gu, arXiv:1907.10018.
[19] C. P. Burgess, J. P. Conlon, L. Y. Hung, C. H. Kom, A. Maharana, and F. Quevedo, J. High Energy Phys. 07 (2008) 073.
[20] L. J. Hall, K. Jedamzik, J. March-Russell, and S. M. West, J. High Energy Phys. 03 (2010) 080.
[21] N. Bernal, M. Heikinheimo, T. Tenkanen, K. Tuominen, and V. Vaskonen, Int. J. Mod. Phys. A **32**, 1730023 (2017).
[22] T. Hambye, M. H. G. Tytgat, J. Vandecasteele, and L. Vanderheyden, Phys. Rev. D **98**, 075017 (2018).
[23] X. Chu, T. Hambye, and M. H. G. Tytgat, J. Cosmol. Astropart. Phys. 05 (2012) 034.
[24] K. Kaneta, Z. Kang, and H. S. Lee, J. High Energy Phys. 02 (2017) 031.
[25] A. Albert *et al.*, Astrophys. J. **834**, 110 (2017).
[26] M. Bauer, P. Foldenauer, and J. Jaeckel, J. High Energy Phys. 07 (2018) 094.
[27] A. Biswas and A. Gupta, J. Cosmol. Astropart. Phys. 09 (2016) 044.
[28] J. Heeck, Phys. Lett. B **739**, 256 (2014).
[29] M. Dutra, M. Lindner, S. Profumo, F. S. Queiroz, W. Rodejohann, and C. Siqueira, J. Cosmol. Astropart. Phys. 03 (2018) 037.
[30] M. Cirelli, P. Panci, K. Petraki, F. Sala, and M. Taoso, J. Cosmol. Astropart. Phys. 05 (2017) 036.
[31] J. L. Feng, I. Galon, F. Kling, and S. Trojanowski, Phys. Rev. D **97**, 035001 (2018).
[32] R. N. Mohapatra and N. Okada, Phys. Rev. D **101**, 115022 (2020).
[33] LEP, ALEPH, DELPHI, L3, OPAL Collaborations and LEP Electroweak Working Group, SLD Electroweak Group, SLD Heavy Flavor Group, arXiv:hep-ex/0312023.
[34] M. Aaboud *et al.* (ATLAS Collaboration), J. High Energy Phys. 10 (2017) 182.
[35] Paul Langacker, Rev. Mod. Phys. **81**, 1199 (2009).
[36] E. W. Kolb and M. S. Turner, Front. Phys. **69**, 1 (1990).
[37] G. Bertone, D. Hooper, and J. Silk, Phys. Rep. **405**, 279 (2005).
[38] N. Aghanim *et al.* (Planck Collaboration), arXiv:1807.06209.

[39] E. Aprile *et al.* (XENON Collaboration), Phys. Rev. Lett. **121**, 111302 (2018).
[40] P. Agnes *et al.* (DarkSide Collaboration), Phys. Rev. Lett. **121**, 081307 (2018).
[41] D. S. Akerib *et al.* (LUX Collaboration), Phys. Rev. D **101**, 042001 (2020).
[42] X. Cui *et al.* (PandaX-II Collaboration), Phys. Rev. Lett. **119**, 181302 (2017).
[43] A. Alves, A. Berlin, S. Profumo, and F. S. Queiroz, J. High Energy Phys. 10 (2015) 076; Phys. Rev. D **92**, 083004 (2015).
[44] E. Del Nobile, M. Kaplinghat, and H. B. Yu, J. Cosmol. Astropart. Phys. 10 (2015) 055.
[45] E. Del Nobile, M. Nardecchia, and P. Panci, J. Cosmol. Astropart. Phys. 04 (2016) 048.
[46] P. Panci, Adv. High Energy Phys. **2014**, 1 (2014).
[47] T. Li, S. Miao, and Y. F. Zhou, J. Cosmol. Astropart. Phys. 03 (2015) 032.
[48] T. Bringmann, F. Kahlhoefer, K. Schmidt-Hoberg, and P. Walia, Phys. Rev. Lett. **118**, 141802 (2017).
[49] T. Hambye, M. H. G. Tytgat, J. Vandecasteele, and L. Vanderheyden, Phys. Rev. D **100**, 095018 (2019).
[50] S. Alekhin *et al.*, Rep. Prog. Phys. **79**, 124201 (2016).
[51] T. Akesson *et al.* (LDMX Collaboration), arXiv:1808.05219.
[52] M. J. Dolan, T. Ferber, C. Hearty, F. Kahlhoefer, and K. Schmidt-Hoberg, J. High Energy Phys. 12 (2017) 094.
[53] P. Ilten, J. Thaler, M. Williams, and W. Xue, Phys. Rev. D **92**, 115017 (2015).
[54] P. Ilten, Y. Soreq, J. Thaler, M. Williams, and W. Xue, Phys. Rev. Lett. **116**, 251803 (2016).
[55] A. Ariga *et al.* (FASER Collaboration), Phys. Rev. D **99**, 095011 (2019).
[56] M. Bauer, P. Foldenauer, and J. Jaeckel, J. High Energy Phys. 07 (2018) 094.
[57] S. Heeba and F. Kahlhoefer, Phys. Rev. D **101**, 035043 (2020).